

Thermal Characteristics of Narrow Gap GMA Welding at Vertical Position with Arc Swinging and Shifting



Hu Lan, Huajun Zhang, Jinjun Shao, Gang Li, Rui Pan, and Bin Wang

Abstract Research on thermal characteristics is the base for deeply understanding the process of narrow gap–fine wire–gas protection–one pass one layer–arc swinging and shifting–vertical welding. The plane analytic geometry method is adapted to solve the arc speed and welding line energy by analyzing the arc movement path. Based on classic heat source model of double ellipsoid, update of arc center position and orientation is achieved by coordinate transformation. The dynamic evolution of the weld pool under certain conditions is simulated, and thermal cycle curves of single layer and multilayer are extracted. The results show that the line energy of the process is pulsed and alternately assigned to both sides of the side wall, which lead to a narrow coarse-grained heat-affected zone (CGHAZ). The thermal cycle curve of CGHAZ presents the double characteristic of multi-peak, dwell time at high temperature is short, and cooling rate at low temperature is low. In addition, the weakest CGHAZ in the joint transforms into several micro-zones along the thickness of the weld, and the area ratio of reheated CGHAZ by normalizing, incomplete normalizing, and tempering is 3:2:5. If the thickness of the welding layer is properly controlled, the original CGHAZ of base metal are subjected to the grain refinement under the different layer welding thermal cycles conditions.

Keywords Narrow gap welding · Vertical welding · Arc swinging and shifting · Coarse-grained heat-affected zone · Welding thermal cycle

H. Lan · J. Shao · G. Li · R. Pan · B. Wang

Key Laboratory of Urban Rail Transit Intelligent Operation and Maintenance Technology & Equipment of Zhejiang Province, Zhejiang Normal University, Jinhua, Zhejiang 321005, China

H. Lan (✉)

Rongcheng Campus, Harbin University of Science and Technology, Rongcheng 264300, Shandong, China

e-mail: lanhu@zjnu.edu.cn

H. Zhang

Technology Department, Shanghai Zhenhua Heavy Industries Co., Ltd, Shanghai 200125, China

© Springer Nature Singapore Pte Ltd. 2020

S. Chen et al. (eds.), *Transactions on Intelligent Welding Manufacturing*,

Transactions on Intelligent Welding Manufacturing,

https://doi.org/10.1007/978-981-15-7215-9_7

1 Introduction

With the development of major national projects and modern industrial equipment toward high capacity and high parameters, the application of large-scale, heavy-duty, high-strength, and thick-plate metal structures is becoming more and more widespread [1]. However, large size and large wall thickness structures (pieces) are difficult to supply for the entire segment, so manufacturing through connection methods has become the first choice. Narrow gap gas shielded welding (NG-GMAW) is an efficient connection method. With the technical advantages of reducing the deposition amount and saving manufacturing time, it has wide application prospects in the manufacture of large-thickness members [2]. In order to ensure the uniform and reliable fusion of the two side walls during the NG-GMAW process, the key to solving this problem is to make the arc center with a higher energy density. Reasonably, close to the side wall of the angle of the zero-inclined bevel, swinging arc, rotating arc, shaking arc, and other technologies have been proposed and applied to NG-GMAW [3, 4]. Researching the heat in the arc swinging (or/and rotating) process characteristics are an important basis for deep understanding of narrow gap-filament-layer-to-layer-gas shielded welding process.

As we all know, the thermophysical properties of the NG-GMAW process will have an important impact on the thermal and metallurgical processes of its joints. The thermal characteristics of the gap-filament-layer-one-layer-swing-arc-arc-gas shielded welding dynamic process are more complex than conventional non-swing (straight through) or small swing amplitude (≤ 3 mm) arc welding. At present, there is not much research on the characteristics of heat dissipation, mainly concentrated in scientific research institutions such as Harbin Institute of Technology, Wuhan University, Lanzhou University of Technology, Jiangsu University of Science and Technology, and Guangdong Institute of Welding Technology [5–7]. Zhang et al. [8, 9] by establishing a heat source model of narrow gap-thick wire-one layer two-pass-submerged arc welding, the temperature field of single-wire and double-wire narrow gap submerged arc welding (NG-SAW) temperature fields is simulated and found that the difference in wire attitude forms different temperature field. They also analyzed the temperature distribution characteristics of the single- and double-filament NG-SAW side wall coarse-grained heat-affected zone (CGHAZ) from the perspective of the corresponding relationship between the temperature field and the tissue transformation. Guo-xiang et al. [10] established a three-dimensional model that simulates the narrow gap-filament-layer-one-layer-swing arc-gas shielded welding temperature field and pool flow and found that there is a large vortex in the entire cross section of the pool. The flow of the molten pool is beneficial to the increase of the penetration depth of the side wall, and the width of the high-temperature area around the molten pool is smaller than that of conventional non-swing arc welding. The above research results are of great significance for the study of the thermal characteristics of the narrow gap-filament-gas protection-one-layer-one-swing-swing arc-vertical welding process.

In this paper, the analytical arc method and numerical analysis methods are used to analyze the arc welding process of the narrow gap swing arc GMA (NG-S²GMA) robot vertical welding and simulate the dynamic evolution of the welding pool. Based on the welding temperature field and thermal cycle curve, we reveal the thermal characteristics of the narrow gap-filament-gas protection-one-layer-one-swing-swing arc-vertical welding process. It is of great scientific significance and engineering application value to lay the foundation for ensuring the optimal thermal process and the best joint performance of NG-S²GMA robot vertical welding of key structures with large thickness.

2 Experiment

The core equipment of the NG-S²GMA robot vertical welding system—the welding head—uses a patented product from Japan’s Babcock-Hitachi Co., Ltd. (Fig. 1), which has linear movement, lateral swing, radial rotation, and composite action functions (all driven by servomotors), which can realize the efficient welding of thick-walled structural parts with a groove clearance of 18–20 mm and a groove depth of 200 mm. Different from the traditional multilayer and multi-channel filling method used in thick-plate vertical welding, NG-S²GMA robot vertical welding adopts multilayer single-channel (one per layer) vertical welding method. The groove depth direction moves in a straight line, while the groove width direction movement is realized by the rotation and swing mechanism of the narrow gap head. The pre-curved section with a length of about 14–15 mm and an angle of 14°–15° with the

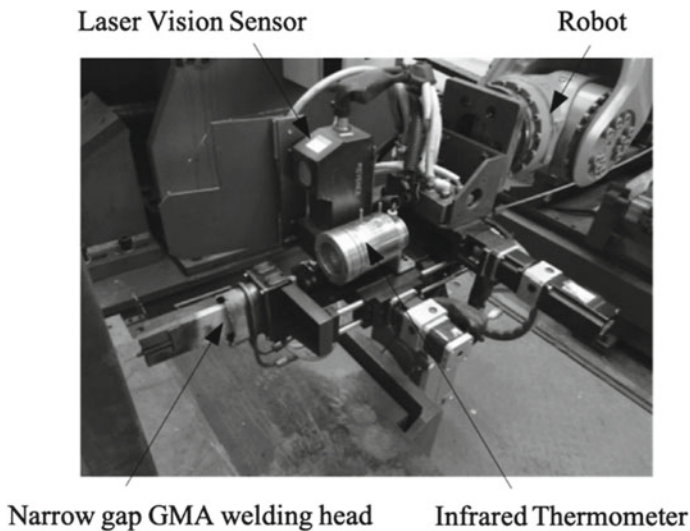


Fig. 1 Welding torch of NG-S²GMA at vertical position

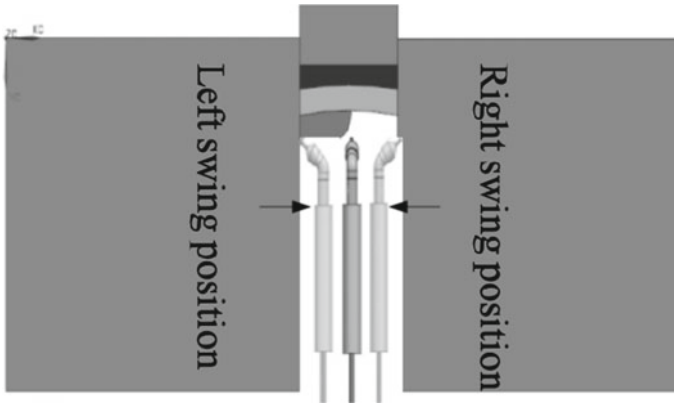


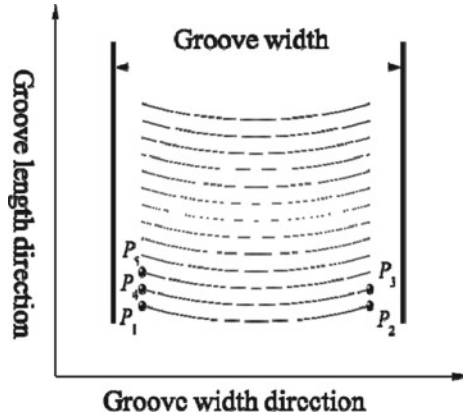
Fig. 2 Top view of NG-S²GMA at vertical position

vertical rod axis is prefabricated at the front end of the conductive rod (the end connected to the conductive tip) so that the orientation of the wire tip changes. When the servomotor on the narrow gap head drives the conductive rod to reciprocate radial rotation, the wire tip (that is, the center of the arc) will rotate around the rod with a constant radius, and the direction of the arc will change periodically. In order to avoid excessive wire feeding resistance and excessively fast arc rotation, which affects the stability of the welding process and also takes into account the convenience of manual adjustment of the distance between the wire end and the groove side wall, the actual welding operation is often the arc rotating around the rod and lateral swing. It should be pointed out that the two sets of back and forth movements of rotation and swing are always synchronized, that is, when the arc moves from the center of the groove to the maximum swing position on both sides of the groove, the arc just rotates around the rod to the maximum rotation angle. The structure shown can obtain stable side wall fusion quality as shown in Fig. 2.

3 Arc Moving Process Analysis and Line Energy Calculation

Accurate control of the spatial position and orientation of the arc is the key to ensuring good fusion of the side walls of the NG-S²GMA robot vertical welding groove. The movement path of the NG-S²GMA robot vertical welding arc is shown in Fig. 3. It is not difficult to see that a complete arc movement process includes the arc's swing movement ($P_1 \rightarrow P_2$ and $P_3 \rightarrow P_4$) between the side walls of the groove (width direction of the groove) and the arc along the length of the groove when the swing is stopped to make a single linear movement ($P_2 \rightarrow P_3$ and $P_4 \rightarrow P_5$). That is to say, the movement speed of the NG-S²GMA robot vertical welding arc is intermittent,

Fig. 3 Arc trajectory of NG-S²GMA at vertical position

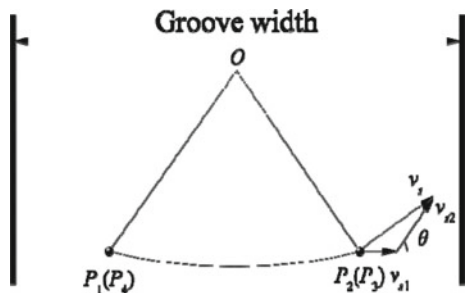


and its size and direction change periodically with the spatial position of the arc, which is different from the conventional non-swing gas shielded welding.

It is well known that the calculation formula of welding line energy is $E = UI/v$ which is determined by the welding speed (or arc moving speed) when the welding current and arc voltage are constant. If you want to qualitatively or quantitatively analyze the thermal characteristics of the narrow gap-filament-gas shield-layer-by-layer-rotary pendulum arc-vertical welding process, you need to accurately calculate the speed of the arc along the moving path in Fig. 3. Among them, $P_2 \rightarrow P_3$ and $P_4 \rightarrow P_5$ are a single linear movement section, and the moving speed of the arc v_r is equal to the moving speed of the end of the robot wrist, and its size and direction remain unchanged. While the two sections $P_1 \rightarrow P_2$ and $P_3 \rightarrow P_4$ are swing pendulum movements, the moving speed of the arc is synthesized by the lateral swing speed and radial rotation speed (linear speed) (Fig. 4). The angle of the speed direction has been changing, which can be expressed as:

$$\theta = \begin{cases} \theta_{\max} - \omega \cdot \text{mod}(\frac{t}{T}) & \text{mod}(\frac{t}{T}) < \frac{T}{2} \\ \theta_{\max} - \omega \cdot [\text{mod}(\frac{t}{T}) - (\frac{T}{2})] & \text{mod}(\frac{t}{T}) > \frac{T}{2} \end{cases} \quad (1)$$

Fig. 4 Arc speed of NG-S²GMA at vertical position



where $\text{mod}(\frac{t}{T})$ is the remainder function of time, t is the total welding time, T is the arc movement period, $T = 2(t_s + t_r)$, $t_s = \lambda/v_{s1}$, and λ are the amplitude of the lateral swing of the arc 5–7 mm, and the swing stop time of the single-side groove is 1.5–1.8 s; ω is the angular velocity of the arc’s radial rotation around the rod, $\omega = \theta_{\text{max}}/(\pi \cdot t_s)$; θ_{max} is the maximum angle of radial rotation 45°–50°.

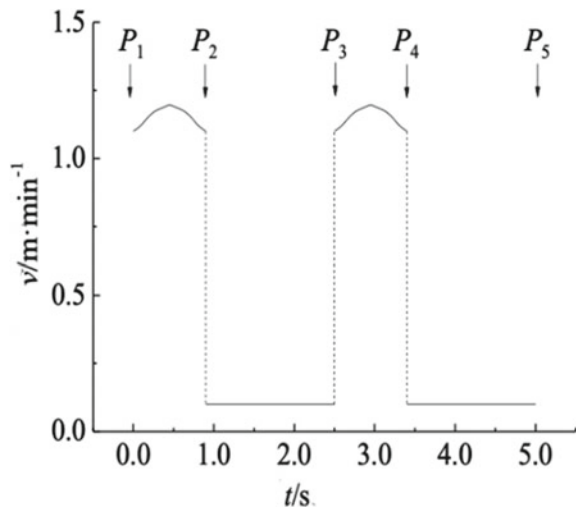
If the angle θ between the lateral oscillating speed v_{s1} and the radial rotational speed v_{s2} is known, the moving speed of the vertical welding arc of the NG-S²GMA robot can be expressed as:

$$v = \begin{cases} v_r & P_2 \rightarrow P_3 \cup P_4 \rightarrow P_5 \\ \sqrt{v_{s1}^2 + v_{s2}^2 + 2v_{s1}v_{s2} \cos \theta} & P_1 \rightarrow P_2 \cup P_3 \rightarrow P_4 \end{cases} \quad (2)$$

In the formula, $v_{s2} = (l_b + l_w) \cdot \omega \cdot \cos \alpha$ l_b, l_w are the parameters that define the radius of rotation of the arc around the rod, l_b is the length of the conductive rod bending section 14–15 mm, l_w is the dry elongation of the welding wire 12–15 mm, α is the conductive rod bending section, and the angle of the rod axis is 14°–15°.

Through experiments, it was found that when the arc’s lateral swing speed $v_{s1} = 0.35 \sim 0.45 \text{ m/min}^{-1}$ along the groove width direction and linear movement speed $v_r = 0.09 \sim 0.10 \text{ m/min}^{-1}$ along the groove length direction, the NG-S²GMA robot’s vertical welding process has good stability, and the weld seam is beautifully formed and slightly concave. At this time, the speed–time curve of the vertical welding arc of the NG-S²GMA robot in one cycle calculated by Eqs. (1) and (2) is shown in Fig. 5. Obviously, the movement speed of the arc shows a “pulse” characteristic. The speed of the “peak” swing section ($v \approx 1.10 \sim 1.20 \text{ m/min}^{-1}$) exceeds the speed of the “base value” linear section ($v \approx 0.10 \text{ m/min}^{-1}$) by more than ten times, and the “duty cycle” is about 0.4. As mentioned above, while keeping

Fig. 5 Variation of arc speed in robotic NG-S²GMA welding at vertical position



the arc power constant, the linear energy of the NG-S²GMA robot’s vertical welding arc is opposite to the change law of the arc moving speed; that is, the swing pendulum segment can be regarded as the “base value” of the pulse line energy. The straight-line segment is the “peak value” of the pulse line energy. The national standard GB/T 3375-94 positions the welding speed as the length of the weld completed in a unit of time, from which the arc line energy in half or one cycle is calculated as:

$$E = \frac{UI}{v_r} \cdot \frac{t_r + t_s}{t_r} \tag{3}$$

Considering that the length of the trajectory l_s of the swing welding arc of the NG-S²GMA robot’s vertical welding arc is about four times the length of the straight line trajectory l_r , it may be possible to calculate the arc energy according to the actual motion trajectory in segments and express it as:

$$E' = \frac{UI}{v_r} \cdot \frac{t_r}{t_r + t_s} + \frac{UI}{v_s} \cdot \frac{t_s}{t_r + t_s} \tag{4}$$

In the formula, v_s is the combined speed of arc swing pendulum $1.10 \sim 1.20\text{m}/\text{min}^{-1}$. Divide Eqs. (3) and (4) to get:

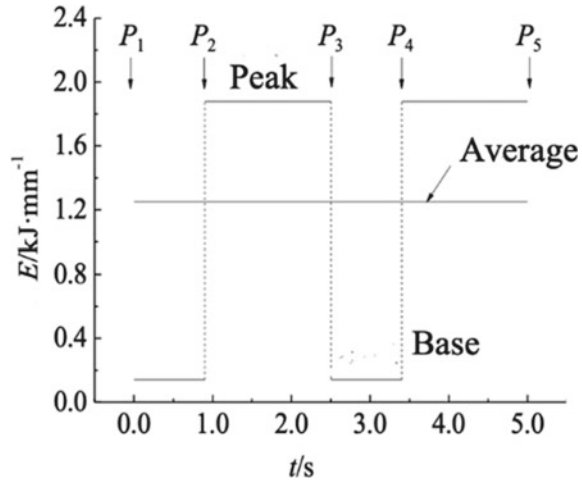
$$\frac{E}{E'} = \frac{v_s}{t_r} \cdot \frac{(t_r + t_s)^2}{v_s t_r + v_r t_s} \approx 2.3 \tag{5}$$

From the calculation result of Eq. (5), the arc energy calculated by method 2 is less than half of method 1. In order to confirm the rationality of the above two-line energy calculation methods, try high-quality offshore engineering steel (advanced low alloy quenched and tempered high-strength steel Q690E) NG-S²GMA robot vertical welding (No. 1-1[#]) and conventional non-swing arc GMA robot vertical welding (No. 1-2[#] and 1-3[#]) heat-affected zone width comparison test. During the test, the distance between the end of the welding wire (the center of the arc) and the side wall of the groove and the direction of the arc remain unchanged. The measurement results of the width of the joint heat-affected zone (excluding the high-temperature tempering zone) under different specifications are shown in Table 1. It can be clearly seen from Table 1 that as the line energy increases ($12.1 \rightarrow 24.1 \text{ kJ}/\text{cm}^{-1}$), the width of the heat-affected zone of the base material side wall increases ($1.8 \rightarrow 2.4 \text{ mm}$). The existing research results show that it is not the total

Table 1 Width of HAZ in vertical GMA welding under different processes

	I (A)	U (V)	V (m/min^{-1})	θ ($^\circ$)	λ (mm)	t_s (s)	E (kJ/cm^{-1})	W (mm)
1-1 [#]	125	22.5	0.09	45	6	1.6	12.5	1.8
1-2 [#]	125	22.5	0.14	–	–	–	12	1.8
1-3 [#]	125	22.5	0.07	–	–	–	24.1	2.4

Fig. 6 Variation of weld heat input in robotic NG-S²GMA welding at vertical position



energy of the arc that actually affects the width of the heat-affected zone of the side wall, but the heat input of the arc to the side wall. The width of the heat-affected zone of the NG-S²GMA robot vertical welding (1-1[#]) is the same as the width of the heat-affected zone of the (1-2[#]) joint using the conventional non-swing arc GMA robot vertical welding. The heat input of the base material side wall under the two-process specifications is basically the same ($\sim 12 \text{ kJ/cm}^{-1}$). Using Eq. (4), it is reasonable to calculate the line energy according to the arc movement path in sections (Fig. 6).

It is worth noting that the total arc energy of the NG-S²GMA robot vertical welding is cyclically transferred to the side wall of the base material on both sides, and the fusion of the side walls of the groove is “time-sharing” rather than synchronized. The heat required for side wall fusion mainly comes from the “peak value” of the pulse arc line energy. The “base value” plays a good role in preheating and post-heat slow cooling. In addition, the width of the heat-affected zone of the (1-1[#] and 1-2[#]) joints is 1.8 mm, indicating that only 2/3 of the pulse arc energy “peak” of the NG-S²GMA robot vertical welding process on the side wall of the base material. The lower side wall heat input is beneficial to the damage of base metal strength, plasticity, and toughness, especially advanced high-strength steel and ultra-high-strength steel. Regarding the whereabouts of residual energy and what kind of joint forming characteristics will be produced by the intermittent arc movement process, further research and analysis of the dynamic evolution of the weld pool is needed.

4 Analysis of Evolution of Molten Pool Morphology and Joint Forming Characteristics

In view of the fact that high-speed camera is not suitable for the monitoring of deep and narrow working conditions approaching zero bevel angle, the paper uses a computer to simulate the dynamic evolution process of narrow gap–fine wire–gas

protection—one pass one layer—arc swinging and shifting—vertical welding. The heat source model uses a double-ellipsoid heat source model, and the heat flux distribution function of the front half ellipsoid can be expressed as [11]:

$$q_f(x, y, z) = \frac{6\sqrt{3}f_f Q}{abc_1\pi\sqrt{\pi}} \exp\left\{-3\left(\frac{x^2}{a^2} + \frac{y^2}{b^2} + \frac{z^2}{c_1^2}\right)\right\} \quad (6)$$

The heat flux density distribution function of the second half ellipsoid can be expressed as:

$$q_r(x, y, z) = \frac{6\sqrt{3}f_r Q}{abc_2\pi\sqrt{\pi}} \exp\left\{-3\left(\frac{x^2}{a^2} + \frac{y^2}{b^2} + \frac{z^2}{c_2^2}\right)\right\} \quad (7)$$

In the formula, a, b, c_1, c_2 is the coefficient that defines the shape of the heat source; f_f, f_r is the energy distribution coefficient that defines the front and rear hemispheres; $f_f + f_r = 2$ generally takes $f_f = 0.6, f_r = 1.4$; Q is the total power of the arc heat source, $Q = \eta UI$, and η is the thermal efficiency coefficient.

The moving process of the vertical welding arc of the NG-S²GMA robot can be regarded as the continuous updating process of the spatial position and direction of the arc center (end of the welding wire) in the groove. Similar to the method described in [12], the movement process of the arc along the path ($P_1 \rightarrow P_2 \rightarrow P_3 \rightarrow \dots$) in Fig. 3 is simulated by the segmented coordinate transformation method. The dynamic evolution of the molten pool morphology is shown in Fig. 7. It is not difficult to see that it is different from the synchronous fusion of the two side walls of the groove during conventional gas welding with no swing or small swing amplitude. The side welding of the side walls of the NG-S²GMA robot vertical welding with a groove gap of 18–20 mm is obvious. The fusion process of the one-sided side wall is a linear movement section when the swing is stopped. It confirms the conclusions drawn from the above dynamic analysis of the “intermittent arc movement” and “pulse arc line energy” dynamic processes. Looking at Fig. 7, we can also find that when the arc moves from one side of the groove to the other side of the groove ($P_1 \rightarrow P_2, t = 15\text{--}16$ s), the moving speed of the arc increases rapidly by ten times. Due to the low surface tension, part of the liquid-deposited metal quickly moves with the arc center, and the surface morphology of the molten pool is elongated, which causes the heat input that originally affected the side wall of the base material to shift-dynamic redistribution of the molten pool heat. After that, the arc line energy remained at the base level, the peak temperature of the molten pool continued to decrease (2400 \rightarrow 1900 °C), and the melting depth was shallow. When the arc moves to the other side of the groove ($P_2 \rightarrow P_3, t = 16\text{--}17.5$ s), the swing motion temporarily stops, and the side wall of the base material begins to receive continuous heat input from the peak value of the pulse arc energy. The “tailing” of the molten pool gradually disappears, the volume gradually increases, the peak temperature continues to rise (1900 \rightarrow 2400 °C), the melting depth also increases, and the molten pool basically returns to the shape

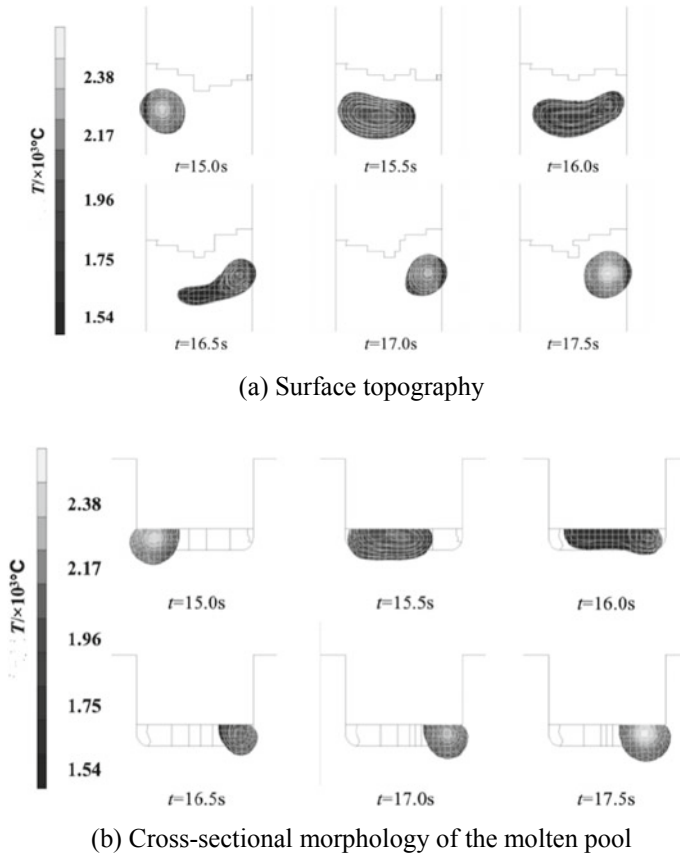
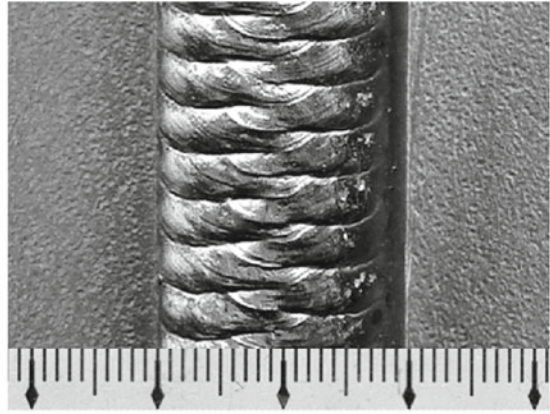


Fig. 7 Evolution of molten pool in robotic NG-S²GMA welding at vertical position

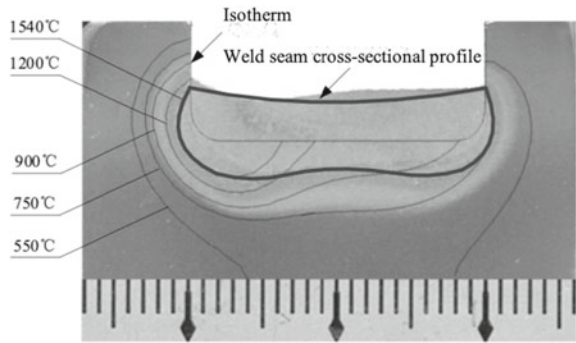
before the swinging movement. That is to say, the main reason for the narrow gap-filament-gas protection-layer-by-layer-swing pendulum arc-vertical welding joint heat-affected zone is the intermittent movement of the arc to cyclically alternate heat input to the base material side wall. The actual joint appearance of Q690E low alloy quenched and tempered high-strength steel NG-S²GMA robot vertical welding is shown in Fig. 8. The surface is formed uniformly and beautifully, the side wall of the base metal is well fused (melting depth ~ 1 mm), the thickness of the welding layer is moderate (3–4 mm), and the welding waveform is like “building blocks” instead of “fish scales,” The cross section of the weld is like a “peanut shell” instead of a “finger,” and the penetration depth between the weld layers is consistent with the change in arc energy. The peak penetration is large (2–3 mm), and the base penetration is small (~ 1 mm). The above joint forming characteristics are the result of the evolution process of the dynamic shape of the molten pool.

As one of the preferred technologies for welding thick-walled structural parts, narrow gap-filament-gas shield-layer-by-layer-swing pendulum arc can obtain a

Fig. 8 Weld appearance of robotic NG-S²GMA welding at vertical position



(a) Weld surface forming



(b) Weld seam cross-sectional profile

narrower base material heat-affected zone (HAZ) through smaller welding line energy. The width of the HAZ of the vertical welding joint of the experimental steel NG-S²GMA robot is basically controlled at about 3 mm, distributed according to the isotherm away from the fusion line (Fig. 7b). HAZ can be divided into coarse-grained heat-affected zone (CGHAZ, 1200–1540 °C), fine-grained heat-affected zone (FGHAZ, 900–1200 °C), dielectric-critical heat-affected zone (ICHAZ, 750–900 °C), and subcritical heat-affected zone (SCHAZ, 550–750 °C). The width ratio of each micro-area is 2:2:1:3 (different from SCHAZ > CGHAZ > FGHAZ > ICAZ in conventional non-swing gas shielded welding). Although the width of CGHAZ is only 1/4 of HAZ (~0.8 mm), the peak temperature of the thermal cycle experienced by this micro-area is high, which is prone to coarsening and embrittlement. As a result, the performance of the micro-zone is “deteriorated” and becomes the “short board” of the entire joint. For the NG-S²GMA robot vertical welding, what kind of thermal process has CGHAZ experienced? This is the basic premise for analyzing the evolution of the structure and performance of the test steel CGHAZ.

5 Analysis of Thermal Cycle Curve in Coarse-Grained Region and Transformation of Micro-Region

In order to reveal the thermal characteristics of the narrow gap-filament-gas shield-layer-by-layer-swing-arc-arc-vertical welding process, the CGHAZ temperature curves of GMA vertical welding joints under different specifications were obtained (Fig. 9). It can be clearly observed from Fig. 9 that, unlike the “single-peak” thermal cycle curve formed by conventional non-swing arc GMA robot vertical welding (2-2[#] and 2-3[#]), NG-S²GMA robot vertical welding (2-1[#]) presents a “multi-peak” characteristic. It consists of a “primary peak” and multiple “secondary peaks” immediately adjacent to it. Statistics show that the time interval between adjacent peaks–peaks (or troughs–troughs) on the thermal cycle curve 2-1[#] is exactly the arc movement period (~5 s). It shows that the crest is caused by the arc approaching the side wall of the base material (temperature measurement point) successively during the intermittent reciprocating movement in the groove, and the trough is formed by the arc gradually away from the side wall of the base material (temperature measurement point). Therefore, “multi-peak” can be regarded as an inherent thermophysical characteristic of swing arc welding. However, the thermal cycle characteristic parameters (such as high-temperature residence time, cooling time) of the multi-peak curve (2-1[#]) and single-peak curve (2-2[#] and 2-3[#]) are quite different. The test conditions and statistical results are listed in Table 2.

Fig. 9 Heat cycle curves of CGHAZ in vertical GMA welding under different processes

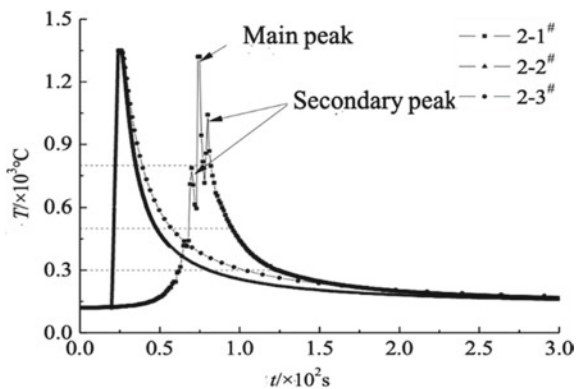


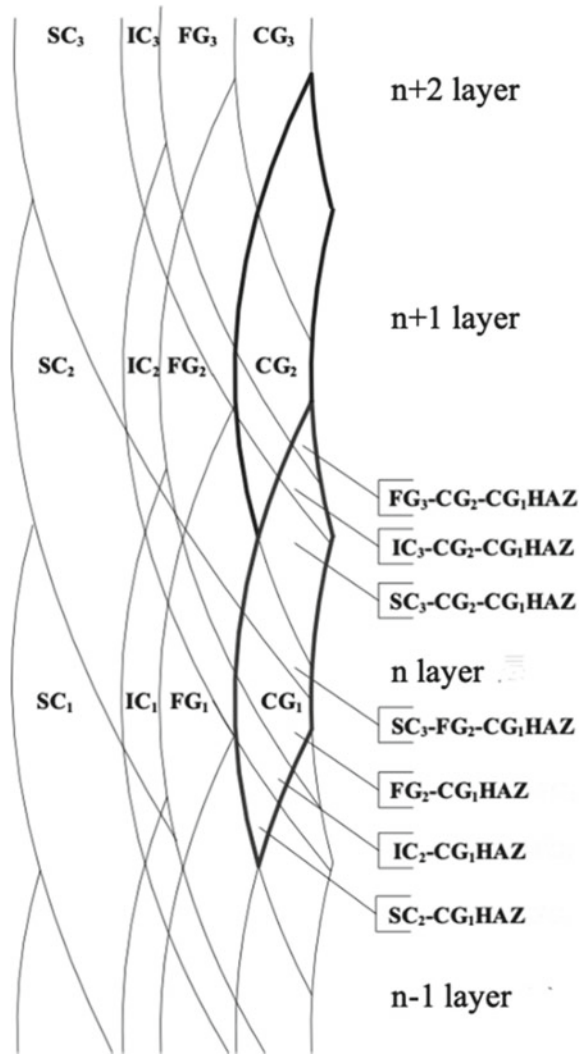
Table 2 Cooling rate of CGHAZ in vertical GMA welding under different processes

	T_0 (°C)	E (kJ/cm ⁻¹)	Interval time		
			t_H	$t_{8/5}$	$t_{8/3}$
2-1 [#]	120	12.5	1.5	17.6	45.8
2-2 [#]	120	24.1	4.9	13	45.8
2-3 [#]	120	32.6	6	18.3	64.1

Comparing the thermal cycle curve parameters calculated in Table 2 found that under the same cooling time, the line energy of the NG-S²GMA robot vertical welding (2-1[#]) is about the half of the conventional non-swinging arc GMA robot vertical welding (2-2[#]). The high-temperature residence time of 2-1[#] CGHAZ is also less than 1/3 of 2-2[#]. However, the cooling time $t_{8/5}$ of 2-1[#] exceeds 2-2[#] 4.6 s. Similarly, under the same cooling time, the line energy of 2-1[#] is less than 2/5 of 2-3[#]. The high-temperature residence time above 1200 °C is only 1/4 of 2-3[#]. This shows that the NG-S²GMA robot vertical welding can obtain a slower cooling rate through a smaller line energy, which is conducive to improving the cold crack resistance of the joint. The high-temperature residence time of CGHAZ is short, which is helpful to avoid the structure being too thick and improves the thermal crack resistance of the joint; that is, the NG-S²GMA robot vertical welding process has good comprehensive crack resistance. The analysis believes that the forming process of the “building blocks” (thickness 2.5–3 mm) of the joint is strong evidence of the “pulsed” characteristics of the heat input of the base material side wall. From the perspective of the effect of heat, the superposition process of three “building blocks” on the side next to the temperature measurement point corresponds to the three valleys of the thermal cycle curve → the peak temperature rise section. On the other side of the bevel, the “building blocks” superimposed on the above three “building blocks” correspond to the peak → valley cooling section. In other words, the “main peak” of the thermal cycle curve is generated when the “building blocks” are stacked close to the temperature measurement point, and the pause time of the arc swing is approximately equal to the high-temperature residence time. The two “building blocks” superimposed are similar to the preheating of the front arc to the rear bead in double-arc welding, and the three “building blocks” superimposed thereafter are similar to the post-heating of the rear arc to the previous bead in double-arc welding. In Fig. 9, the three trough temperatures formed by the superposition of “building blocks” on the opposite side of the temperature measurement point are 596, 715, and 750 °C, respectively. Multiple pulse preheating and post-heating have played a good slow cooling effect.

The thick-walled component NG-S²GMA robot vertical welding adopts a multi-layer single-pass filling method, and the rear weld bead (layer) is bound to have a thermal effect on the previous weld bead (layer) and HAZ. The welding layer of NG-S²GMA robot vertical welding head is relatively thin (3–4 mm), and the penetration depth of the welding seam when the arc swing is paused is large (2–3 mm). This means that the thickness of the arc heat action exceeds 5 mm, and basically, the current layer of weld beads will affect the previous two layers of weld beads. In other words, the base material side wall CGHAZ will undergo reheating processes such as normalizing, incomplete normalizing, and tempering of the rear weld bead (layer). The thermal cycle curve shows the dual characteristics of “multi-peak,” and the organization and performance of the micro-area change accordingly. Taking the welding layer thickness of 3.5 mm as an example, the thermal process of the multi-layer vertical welding of the NG-S²GMA robot is simulated by superimposing the HAZ isotherms during single-layer vertical welding. The isotherm distribution and micro-zone division of the CGHAZ of the base material side wall are obtained as shown in Fig. 10. In order to distinguish the description, each micro-area is described

Fig. 10 Evolution of CGHAZ in robotic NG-S²GMA welding at vertical position



with English letters and Arabic numerals. Arabic numerals represent the number of welding thermal cycles experienced by CGHAZ. Observe the distribution of the HAZ isotherms shown in Fig. 10, and CGHAZ of the base metal side wall corresponding to each weld is shaped like a “big knife” (the thick red line and the blue thick line mark the part). When the weld of the $n + 1$ layer is completed, the base material CGHAZ of the n layer has experienced secondary overheating, normalizing, incomplete normalizing, and tempering from top to bottom. It is transformed into four micro-zones, namely CG₂-CG₁HAZ, FG₂-CG₁HAZ, IC₂-CG₁HAZ, and SC₂-CG₁HAZ. The proportion of the area of each micro-zone is 40, 39, 12, and 9%. When the $n + 2$ layer weld is completed, CG₂-CG₁HAZ is transformed into three

micro-zones (FG3-CG2-CG1HAZ, IC3-CG2-CG1HAZ, and SC3-CG2-CG1HAZ), and the proportion of the area of each micro-zone is 4, 8, and 28%. FG2-CG1HAZ transforms into two micro-zones (SC3-FG2-CG1HAZ and FG2-CG1HAZ), which occupy about 16 and 23% of the area. In short, after undergoing the reheating effect of the rear weld bead (layer), the weakest CGHAZ in the vertical welding joint of the NG-S²GMA robot forms several micro-areas along the thickness direction of the weld. Experience normalizing (FG3-CG2-CG1HAZ and FG2-CG1HAZ), incomplete normalizing (IC3-CG2-CG1HAZ and IC2-CG1HAZ), and tempering (SC3-CG2-CG1HAZ, SC3-FG2-CG1HAZ, and SC2-CG1HAZ), the area ratio of the micro-area is 3:2:5. Moreover, if the thickness of the welding layer is properly controlled, the original CGHAZ of the base material is basically eliminated. This shows that the NG-S²GMA robot vertical welding process itself has the function of optimizing the joint structure and performance. However, due to the different reheat processes experienced by each transition micro-region, its organization and performance improvement mechanisms and effects are also different, and further research is needed.

6 Conclusion

1. Due to the intermittent movement of the arc, the narrow gap–fine wire–gas protection–one pass one layer–arc swinging and shifting–vertical welding line energy changes are pulse characteristics. The heat required for the fusion of the base material side wall comes from the peak value of the pulse arc line energy.
2. Narrow gap–fine wire–gas protection–one pass one layer–arc swinging and shifting–vertical welding total energy are distributed alternately to the side wall of the base material on both sides. The side wall thermal cycle curve has multi-peak characteristics, residence time at high temperature is short, cooling rate at low temperature is slow, and heat influence zone of coarse crystal is narrow.
3. The weakest coarse-grained heat-affected zone in the joint is transformed into several micro-zones along the thickness of the weld by the reheating effect of multilayer welding. The original coarse-grained heat-affected zone is basically eliminated, but the structure and performance of each transition micro-zone are different, and the improvement mechanism is also different.

References

1. Wang P, Liu X, Lu F-g (2016) Application of deep-narrow gap welding method in manufacturing component with heavy section. *J Mech Eng* 52(2):56–61
2. Zheng Y-w, Cai Z-p, He Y-c et al (2016) Study on the influence of fusion ratio on carbon migration phenomenon in the narrow gap welding of dissimilar steels. *J Mech Eng* 52(12):74–80

3. Zhang F-j, Guo J-l, Zhang G-d (2017) Key technologies of narrow gap gas shielded arc welding. *Electr Weld Mach* 47(7):30–33
4. Lan H, Zhang H-j, Chen S-b et al (2014) Correlation of arc sound and arc-sidewall position in narrow gap MAG welding. *J Mech Eng* 50(12):38–43
5. Li W-h, Gao K, Wang J-y et al (2015) A vision sensing based welding deviation detection algorithm for rotation arc narrow gap MAG welding. *J Shanghai Jiao Tong University* 49(3):353–356
6. Xu W-h, Lin S-b, Yang C-l et al (2017) Study on droplet transfer of swing arc narrow gap GMAW. *Trans China Weld Inst* 38(2):109–114
7. Gu Y-f, He G-y, Shi Y et al (2016) Detection and analysis of arc shape and droplet transfer behavior of narrow gap GMAW. *J Shanghai Jiao Tong University* 50(10):1526–1534
8. Zhang L, Liu C-q, Yu J-w et al (2016) Numerical analysis of temperature field of narrow gap submerged arc welding. *Trans China Weld Inst* 37(3):83–87
9. Zhang L, Liu C-q, Yu J-w et al (2016) Numerical analysis of microstructure evolution of coarse grained zone in sidewall during narrow gap submerged arc welding. *Trans China Weld Inst* 37(4):103–106
10. Guoxiang X, Jiayou W, Pengfei L et al (2018) Numerical analysis of heat transfer and fluid flow in swing arc narrow gap GMA welding. *J Mater Process Technol* 252:260–269
11. Ligang W, Jason C, Degala VK et al (2016) CFD simulations of GMA welding of horizontal fillet joints based on coordinate rotation of arc models. *J Mater Process Technol* 231:221–238
12. Lan H, Zhang H-j, Chen A-j et al (2015) Numerical simulation on dynamic process and thermal physical properties of narrow gap MAG vertical welding. *Trans China Weld Inst* 36(7):77–82